Cell, Vol. 116, 431–443, February 6, 2004, Copyright ©2004 by Cell Press

Periodic Lamellipodial Contractions Correlate with Rearward Actin Waves

Grégory Giannone,[1] Benjamin J. Dubin-Thaler,[1] Hans-Günther Döbereiner,[1] Nelly Kieffer,[2] Anne R. Bresnick,[3] and Michael P. Sheetz[1,*]
[1]Department of Biological Sciences
Columbia University
New York, New York 10027
[2]Laboratoire Franco-Luxembourgeois de Recherche Biomedicale
CNRS/CRP-Sante
University Center
162A Avenue de la Faiencerie
L-1511 Luxembourg
[3]Department of Biochemistry
Albert Einstein College of Medicine
1300 Morris Park Avenue
Bronx, New York 10461

Summary

Cellular lamellipodia bind to the matrix and probe its rigidity through forces generated by rearward F-actin transport. Cells respond to matrix rigidity by moving toward more rigid matrices using an unknown mechanism. In spreading and migrating cells we find local periodic contractions of lamellipodia that depend on matrix rigidity, fibronectin binding and myosin light chain kinase (MLCK). These contractions leave periodic rows of matrix bound β3-integrin and paxillin while generating waves of rearward moving actin bound α-actinin and MLCK. The period between contractions corresponds to the time for F-actin to move across the lamellipodia. Shortening lamellipodial width by activating cofilin decreased this period proportionally. Increasing lamellipodial width by Rac signaling activation increased this period. We propose that an actin bound, contraction-activated signaling complex is transported locally from the tip to the base of the lamellipodium, activating the next contraction/extension cycle.

Introduction

During cell spreading and migration, cells extend lamellipodia and encounter new extracellular matrix (ECM) environments. During this active process, the cell probes the chemical nature of the matrix through integrin binding and determines the physical rigidity of the matrix through contractile forces. As a result, chemical composition and rigidity of the matrix are guiding factors in cell motility (Bokel and Brown, 2002) as well as being required for cell growth, viability, and morphogenesis (Huang and Ingber, 1999). Because motility involves the generation of forces, one would expect a coupling between the actin assembly causing membrane extension (Pantaloni et al., 2001; Pollard and Borisy, 2003; Small et al., 2002) and the activity of myosins causing contraction (Mitchison and Cramer, 1996). Indeed, a gradient in ECM stiffness causes fibroblasts to move from soft to stiff substrate (Lo et al., 2000; Mandeville et al., 1997), and lamellipodial extensions are directed by intracellular traction forces (Parker et al., 2002). In no case, however, is the precise mechanism for converting the rigidity of the ECM into a directional signal understood. Contractile force is postulated to cause membrane channel opening (Gillespie and Walker, 2001), the activation of membrane phosphatase-integrin complexes (von Wichert et al., 2003), or the stretching of cytoskeletal proteins (Sawada and Sheetz, 2002). While these force-activated processes provide mechanisms for the local generation of signals, the cell must also transmit these signals to remote myosin contraction complexes or to the nuclear region. To date, no evidence of such remote transmission of local signaling exists.

In vitro studies of actin polymerization have identified critical proteins recruited by pathogens to enable their actin-based movement in host cytoplasm (Loisel et al., 1999; Pantaloni et al., 2001). Thus, there has been recent progress in understanding the mechanism by which actin assembly can power cell edge extension. Recent reviews have summarized some of the current models (Pantaloni et al., 2001; Pollard and Borisy, 2003; Small et al., 2002). The actin network in both the Listeria actin tail and in the lamellipodium has a relatively constant length and a stationary gradient reflecting a steady-state process of assembly at the front and disassembly at the rear (Cameron et al., 2000; Pantaloni et al., 2001). The lamellipodium tip engages protein complexes including Ena/VASP family proteins, Scar/WAVE, N-WASP, and Arp2/3 that increase actin filament nucleation and polymerization. Small GTPases from the Rho family have been linked to this activation step (Miki et al., 2000; Rohatgi et al., 1999). The formation and stabilization of the two-dimensional actin network is achieved by Arp2/3 as well as by actin crosslinking proteins like filamin, α-actinin, and cortactin. Disassembly of the actin meshwork is mediated by ADF/cofilin (Lappalainen and Drubin, 1997) and possibly by severing proteins like gelsolin. The inactivation of cofilin, caused by its phosphorylation by LIM kinase, correlates with the Rac-induced production of lamellipodia (Arber et al., 1998; Yang et al., 1998) and illustrates the tight link between assembly at the front and disassembly at the rear that sets lamellipodial width.

In model systems such as pathogens, the reduction of the motility process to its basic components can elucidate the role of individual constituents in cellular motility. However, in order to link the activity of the lamellipodium to complex processes such as cell spreading, migration, and polarization, quantitative analysis of lamellipodial dynamics is required. For example, the cytoskeletal treadmilling cycle can power actin-based movement of beads or bacteria, without the need for myosin-based contractility (Loisel et al., 1999). However, cell contractility is needed for cell spreading (Cramer and Mitchison, 1995) and migration (Munevar et al., 2001). We have recently developed a system for analyzing the complete

*Correspondence: ms2001@columbia.edu

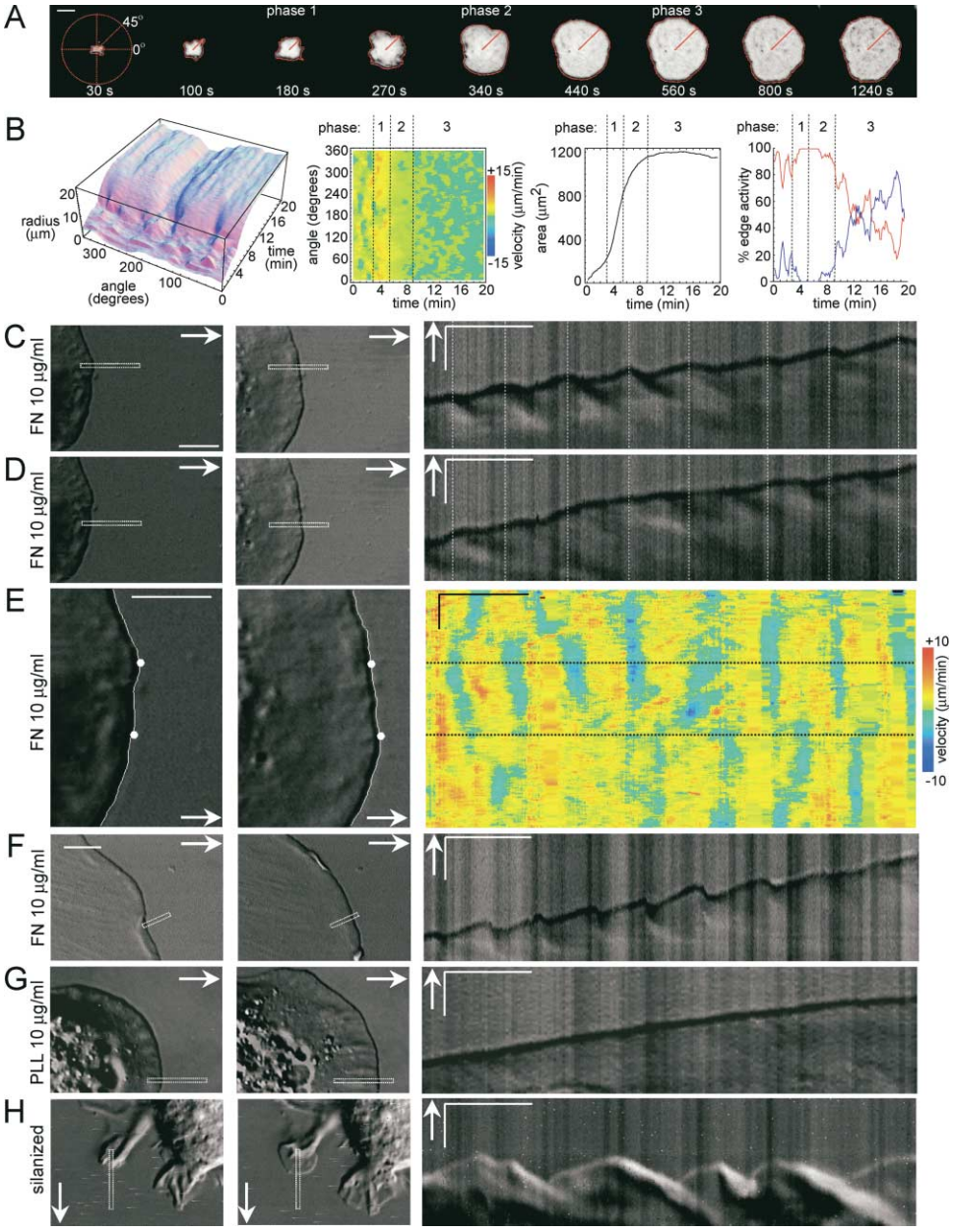

Figure 1. Lamellipodial Extension Is Characterized by Periodic Interruptions

(A) Individual TIRF images of a MEF spreading on FN 10 μg/ml were analyzed by a program that located the outline between the fluorescent cell and the background and expressed this outline in polar coordinates. The distance (red line) from the centroid of the first outline to the outline edge for each frame was determined at evenly spaced angles (1°) around the cell. Scale bars are equal to 10 μm.

(B) Radius as function of angle and time in Cartesian coordinates (left). Radial edge velocity plotted as a function of time and angle, giving a velocity map (middle left). Variation of the cell area during the progression of spreading (middle right). The percent of edge activity (protrusion in red, retraction in blue) was determined by taking the quotient of the active length along the periphery and the total length along the periphery for a given time (right). These representations revealed 3 phases of isotropic spreading cells. Acquisition rate: 1 frame every 5 to 10 s.

(C–D) DIC kymographs of a MEF spreading on FN 10 μg/ml (right). The dotted rectangles in the left (beginning of the kymograph) and middle (end of the kymograph) depict the regions used to generate the DIC kymographs. Note the difference in the phase of interruption/retraction generated between the regions. See Supplemental Movie S1A (available on *Cell* website) to better appreciate the generation of periodic interruptions.

(E) Velocity map of the cell edge detected from a DIC time-lapse. The white lines in the left (beginning of the time lapse) and middle (end of the time lapse) correspond to detection of the cell edge. The white dots correspond to the dotted black lines in the velocity map (right) and to the regions in (C) and (D).

(F) DIC kymograph of a migrating MEF on FN 10 μg/ml. Migrating cells are defined as cells having active lamellipodia and a polarized morphology (trigonal) more than 3 hr after plating. See Supplemental Movie S1B available on *Cell* website.

(G) DIC kymograph of a MEF spreading on poly-L-lysine 10 μg/ml.

(H) DIC kymograph of a MEF spreading on a silanized coverglass.

Left: Scale bars are equal to 5 μm. Right: time bars are equal to 30 s; scale bars are equal to 2 μm. Arrows indicate the direction of protrusion.

process of cell spreading on ECM at a submicron level (Dubin-Thaler et al., 2004), which reveals a surprising stochastic nature to the spreading process.

In slow-migrating cells, like fibroblasts, rounds of protrusion and retraction that lead to membrane ruffling and a small net movement of the cell have been observed (Bear et al., 2002). However, EGF stimulated carcinoma cells (Bailly et al., 1998) or serum-starved spreading fibroblasts (Dubin-Thaler et al., 2004) display faster net movement of the leading edge with few ruffling events, suggesting a continuous movement. An inverse relationship between the speed of the edge protrusion and rearward movement of the actin cytoskeleton has been observed in active lamellipodia (Cameron et al., 2000) and filopodia (Sheetz et al., 1992). This suggests that fast actin retraction compromises the ability of the cell to extend rapidly; however, contraction is needed to apply forces to integrins (Choquet et al., 1997) and probe ECM rigidity during extension.

In this study, we explored how the cell can locally transduce the rigidity of the ECM into a contractile signal used to direct cell edge extension. We discovered a remarkably periodic contraction of lamellipodia without filopodia in spreading and migrating cells that depends upon a stiff substrate, integrin binding, and myosin light chain kinase (MLCK) activation. Our findings support a local cytoskeletal signal transport hypothesis. In that hypothesis, the signal is generated locally by forces applied to a stiff ECM at the tips of lamellipodia and is transported by the actin cytoskeleton to the back of lamellipodia where it activates contraction, starting the next cycle.

Results

Lamellipodial Extension Is Characterized by Periodic Interruptions in Spreading and Migrating Cells

Cell protrusion during spreading or migration on a matrix-coated surface requires an actin-dependent membrane extension, the lamellipodium. Total internal reflection fluorescence (TIRF) microscopy of dye-loaded cells reveals the region of close contact between the cell and the substrate. Integrin-mediated adherence during lamellipodial extension generates close contact of the cell with the ECM and we calculate variations in this region with submicron and second precision (Figure 1A). We analyzed the spreading of mouse embryonic fibroblasts (MEFs) on glass coated with fibronectin (FN) and found that there were two modes of spreading: anisotropic or isotropic (Dubin-Thaler et al., 2004). In anisotropic spreading, extensions are supported by filopodia and are irregular with many stochastic transient extension periods (STEPs). In isotropic spreading, extensions lack filopodia and are nearly continuous until cells are almost completely spread (Figure 1B). Upon closer examination of the isotropic spreading process, we observed periodic interruptions in the lamellipodial extension with a period of about 24 s (Figures 1C–1E). Since this oscillating behavior might reflect local regulation of the lamellipodial extension process under normal conditions, we felt that careful examination of the periodic phenomenon might reveal important mechanisms used by the cell to control motility.

To determine if this periodicity was a general behavior, we analyzed the lamellipodia of polarized migrating MEFs with or without serum. Cells were chosen based upon their polarized (trigonal) morphology and were separately analyzed based upon the presence or absence of filopodia. In lamellipodia lacking filopodia (51 $\pm$ 14% [n = 72 cells] in the absence of serum; 68 $\pm$ 2% [n = 75 cells] with 10% serum) periodic interruptions were observed in most cases (91 $\pm$ 3% [n = 37 cells] without serum; 90 $\pm$ 3% [n = 51 cells] with serum) (Figure 1F). However, in lamellipodia having filopodia (49 $\pm$ 14% [n = 72 cells] without serum; 32 $\pm$ 2% [n = 75 cells] with serum) periodic interruptions were rarely observed (17 $\pm$ 7% [n = 35 cells] without serum; 24 $\pm$ 22% [n = 24 cells] with serum) (Supplemental Figure S1A available at http://www.cell.com/cgi/content/full/116/3/431/DC1). Furthermore, in polarized endothelial cells having lamellipodia without filopodia (55 $\pm$ 16% [n = 73 cells] with serum), periodic interruptions were also observed (93 $\pm$ 7% [n = 39 cells] with serum). Likewise, in lamellipodia with filopodia (45 $\pm$ 16% [n = 73 cells] with serum) periodic interruptions were rarely observed (20 $\pm$ 14% [n = 34 cells] with serum). Periodic interruptions of lamellipodia were also observed during spreading of another MEF cell line and of endothelial cells (Supplemental Figure S1 available on *Cell* website).

To standardize and probe the molecular mechanism of the periodic interruptions we focused on isotropic spreading MEFs. During isotropic spreading we found 3 phases of spreading based on, (1) the dynamics of the leading edge (Figures 1A and 1B), (2) integrin interaction with the rearward actin flow (Figure 2), and (3) the pattern of adhesion sites (Figure 3). In order to view the spreading of the entire cell in one graph, we expressed the distance from the center to the edge of the cell as a function of time and evenly spaced angles around the cell (Figure 1B, left). Edge velocity at a given time was measured by taking the derivative of distance with respect to time. Using color to designate the velocity, a two-dimensional (angle versus time) plot showed the dynamics of the spreading process (Figure 1B, middle left). In the initial phase of spreading (phase 1), there was a fast and nearly global protrusion of the edge at a constant rate. In the second phase, the rate of edge extension decreased (phase 2) and displayed periodic interruptions (Figures 1C–1E). The final, fully spread phase (phase 3) was characterized by two possible cell states. The first state displayed irregular extensions and withdrawals of the lamellipodia (i.e., STEPs similar to anisotropic spreading cells). The second state displayed continuous extensions with periodic interruptions (Figure 1F).

Periodic interruptions were best seen by differential interference contrast (DIC) microscopy in kymographs of the protruding cell edge (Figures 1C, 1D, and 1F). The regular pattern of interruptions was seen in the majority of isotropic spreading cells (87 $\pm$ 13%, n = 62 cells). On average a single cycle, defined as a protrusion followed by a retraction, had a period of 24 $\pm$ 7 s (n = 95 events, 12 cells). The duration of the protrusion was 19 $\pm$ 6 s and the distance traveled by the leading edge before the retraction period was 1050 $\pm$ 480 nm (n = 71 events, 9 cells) giving a mean speed of 50 $\pm$ 17 nm/s (n = 66 events, 9 cells). After the retraction, which lasted

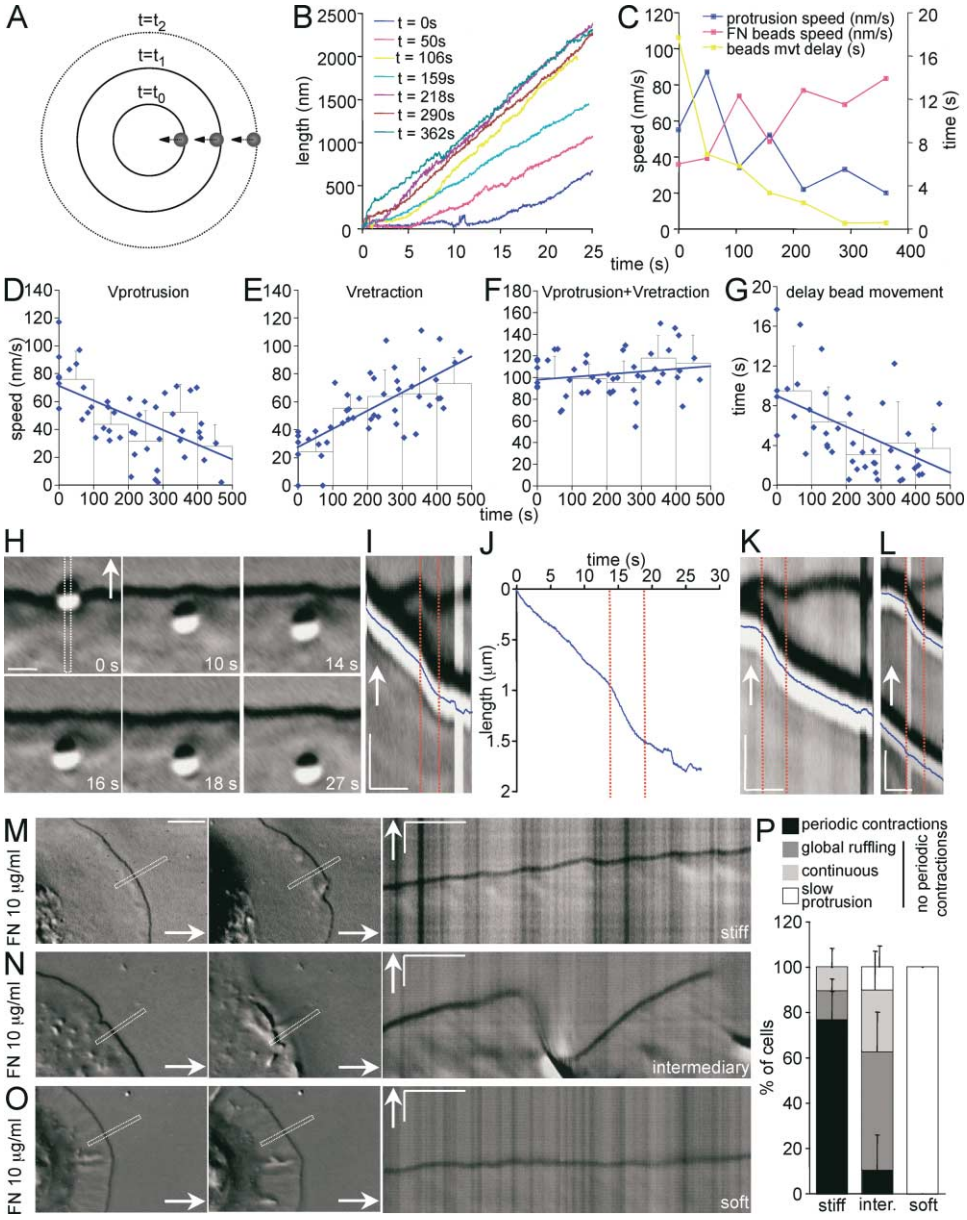

Figure 2. Generation of Periodic Interruptions Correlates with Increased Forces Applied on Integrins

(A) Schematic representation of the laser trap experiment during isotropic MEF spreading. FN-coated beads were sequentially positioned on the tip of the protruding lamellipodium using a laser trap during the progression of spreading.

(B) Displacement versus time plot of a representative experiment showing the movement of restrained FN-coated beads drawn out of the laser trap during isotropic MEF spreading. Color codes specify the time of initial binding of the FN-coated beads. Note the increase in rate and decrease in delay of rearward movement during the progression of spreading.

(C) Plot corresponding to the cell in (B) showing the decrease in the rate of cell protrusion (blue curve), the increase in the rate of FN-coated beads movement (pink curve), and the decrease in the delay of movement (yellow curve).

(D) Velocity of the cell edge protrusions (Vprotrusion); (E) velocity of the FN-coated bead rearward movement (Vretraction); (F) sum of Vprotrusion + Vretraction and (G) delay of bead movements, versus time of initial binding plots. The observed trends in Vprotrusion, Vretraction, Vprotrusion + Vretraction, and in the bead delay time were tested for statistical significance. Slopes of linear fits to the data (Figures 2D–2G) gave quantitative measures of changes over time. At a 99% confidence level, Vprotrusion decreases (-0.11 ± 0.06 nm/s^2); Vretraction increases (0.13 ± 0.05 nm/s^2); Vprotrusion + Vretraction stays constant (0.02 ± 0.06 nm/s^2); and bead delay decreases (-0.02 ± 0.01 s/s).

(H) Time-lapse sequence (see Supplemental Movie S2A available on *Cell* website) used to generate the DIC kymograph (I), depicting the movement of a FN-coated bead and the movement of the cell edge during an interruption event. Note the correlation of the cell edge retraction (between dotted red lines) and the increase in the rate of the FN-coated bead (superimposed blue line) (J). This correlation is observed both if the bead is located close to (K and L, upper bead) or back from (I) the lamellipodium tip, but not on the lamella (L, lower bead). Scale bars are equal to 1 µm. Time bars are equal to 10 s. Arrow indicates the direction of protrusion.

(M) DIC kymographs of a MEF spreading on a stiff polyacrylamide gel (20% acrylamide, 0.8% bisacrylamide) covalently linked with FN 10 µg/ml. Periodic contractions were generated. See Supplemental Movie S2B available on *Cell* website.

(N) DIC kymographs of a MEF spreading on an intermediary stiffness polyacrylamide gel (10% acrylamide, 0.1% bisacrylamide) covalently linked with FN 10 µg/ml. Note the effective protrusion of the leading edge without the generation of periodic contractions and the following global ruffling of the lamella. See Supplemental Movie S2C available on *Cell* website.

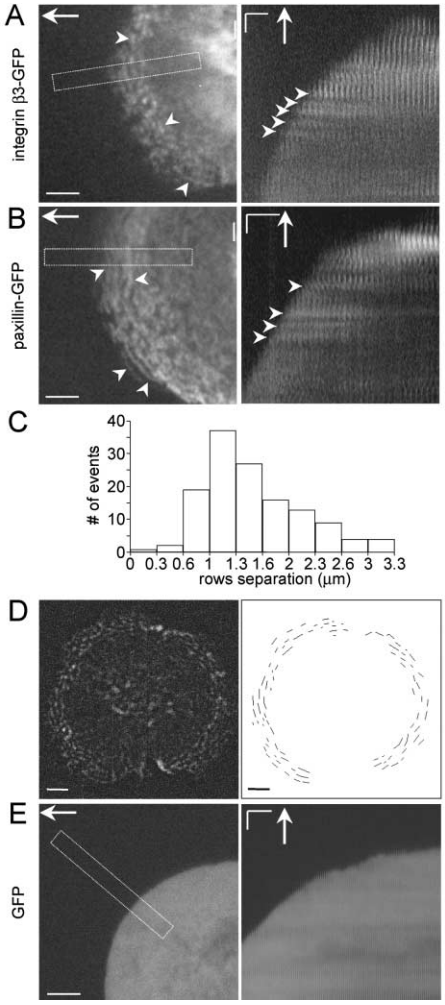

Figure 3. Interruptions/Contractions Induce the Periodic Formation of Transient Integrin and Paxillin Clusters

(A–B) TIRF kymographs of MEFs expressing integrin-β3-GFP (A) or paxillin-GFP (B) spreading on FN 10 μg/ml (right). The dotted rectangles in the left (superposition of 4 successive frames) depict the regions used to generate the TIRF kymographs. Arrowheads indicate the formation of transient rows of integrin-β3-GFP and paxillin-GFP. See Supplemental Movie S3 (available on *Cell* website) to better appreciate the generation of periodic integrin rows during the phase 2 of spreading. Left: scale bars are equal to 5 μm. Right: scale bars are equal to 2 μm. Time bars are equal to 60 s. Arrows indicate the direction of protrusion. Acquisition rate: 1 frame every 10 to 15 s.

(C) Histogram of the distribution of distances between integrin-β3-GFP rows.

(D) Rows were visualized using superposition of consecutives frames (left). Manual localization of integrin rows was performed on the right and distances were analyzed in mathematica. Scale bars are equal to 5 μm.

(E) TIRF kymograph of a MEF expressing GFP spreading on FN 10 μg/ml (right).

for 5 ± 2 s for a distance of 220 ± 130 nm (n = 66 events, 9 cells), the net protrusion distance was 840 ± 520 nm (n = 65 events, 9 cells). Although periodic interruptions were seen around the whole edge of the cell, there was no temporal coordination of adjacent sequences of retraction. Kymographs of closely spaced regions (Figures 1C and 1D), or a velocity map of the leading edge (Figure 1E), showed a similar period with an offset that varied along the cell edge. Thus, the period was constant over the cell but was not globally controlled. In migrating cells with lamellipodia lacking filopodia, periodic interruptions were observed having a period of 21 ± 4 s (n = 124 events, 12 cells) (Figure 1F), close but significantly different from spreading cells (Bonferroni post hoc test).

To determine if the period was dependent on integrin activation and not just binding to the surface, we performed the same analysis on cells spreading on poly-L-lysine (PLL). Unlike cells spreading on FN, the protrusion of the cell edge during the slower second phase was not interrupted by periodic stops (5 cells) (Figure 1G, Supplemental Figure S2 available on *Cell* website). To further examine the role of integrins, soluble RGD peptide was added and was found to block further spreading on the surface (Dubin-Thaler et al., 2004). However, previous studies have shown that cell edge protrusion does not require integrin interaction with the ECM (Bailly et al., 1998). Indeed, most cells plated on a nonadherent, silanized coverglass did not spread, but many cells displayed "spontaneous" protrusions close to the coverglass. Unlike cells on FN-coated glass, these protrusions were entirely withdrawn without a net cell edge movement (Figure 1H). This behavior, protrusion and withdrawal, was similar to the cell edge movement observed in slowly migrating fibroblasts (Bear et al., 2002) and reinforced the idea that FN surfaces directed motility but were not required for it to occur. Furthermore, there was no periodicity to the extension and retraction cycles.

Periodic Interruptions of the Lamellipodial Extension Are Triggered by Increased Actin Rearward Movement from Periodic Contractions

Phase 2 of spreading was characterized by the initiation of a fast rearward movement of actin filaments (Dubin-Thaler et al., 2004), indicating that increased forces were applied to ECM sites by the actin flow. To estimate the rearward movement of lamellipodial actin and the resulting forces exerted on integrins, we analyzed the movement of FN-coated beads bound to the cell surface (Figure 2). Using a laser trap, beads were positioned on the tip of the protruding lamellipodium at different times during the progression of spreading (Figure 2A). We found that at early times in isotropic spreading (<100 s), corresponding to fast lamellipodial protrusion (phase

(O) DIC kymographs of a MEF spreading on a soft polyacrylamide gel (10% acrylamide, 0.04% bisacrylamide) covalently linked with FN 10 μg/ml. Note the absence of both periodic contractions and effective protrusion of the leading edge. See Supplemental Movie S2D available on *Cell* website.

Left: Scale bars are equal to 5 μm. Right: time bars are equal to 30 s; scale bars are equal to 2 μm. Arrows indicate the direction of protrusion.

(P) Histogram representing the percentage of cells displaying periodic contractions (black), global ruffling (dark gray), continuous protrusion (light gray), and slow protrusion (white) for respectively, MEFs spreading on stiff, intermediary, and soft substrate.

1) (76 ± 20 nm/s; n = 13 events, 6 cells) (Figure 2D), restrained FN-beads were drawn out of the laser trap with a large delay (10 ± 5 s) (Figure 2G) and a slow speed (25 ± 15 nm/s) (Figure 2E). During the next period of spreading, the speed of rearward movement of restrained FN-coated beads increased to 56 ± 10 nm/s (e.g., for 100 to 200 s after plating; n = 21 events, 6 cells) and the delay of movement decreased to 6 ± 3 s (Figures 2B and 2C). When the cell reached its final area (phase 3) restrained FN-beads were drawn out of the laser trap rapidly (after >300s, the delay decreased to 4 ± 3 s; n = 18 events, 6 cells) and the speed increased to 71 ± 21 nm/s. The sum of lamellipodia protrusion velocity and rearward transport velocity of beads was essentially a constant during the entire spreading process (105 ± 22 nm/s, n = 52 events, 6 cells) (Figure 2F), suggesting a reciprocal relationship between these two parameters.

The periodic interruptions observed in lamellipodial extension could result either from a decrease in polymerization rate or an increase in the velocity of actin rearward movement. Consequently, we simultaneously followed the movement of the cell edge and FN-coated beads during an interruption (Figures 2H–2L). A transient increase in the velocity of FN-coated beads occurred at the onset of interruptions (difference in t = 0.6 ± 0.5 s; n = 16 events, 7 cells) and the ratio of their durations was close to 1 (duration of periodic interruptions was 5.3 ± 1.8 s versus 5.2 ± 1.9 s for velocity increases; ratio 1 ± 0.1; n = 16 events, 7 cells). Furthermore, the increase in retraction rate was observed for FN-coated beads close (Figures 2K and 2L, upper bead) or back from (Figure 2I) the edge of the lamellipodium but not for beads more distant on the lamella (Figure 2L, lower bead). In addition, the sum of the rearward movement of FN-coated beads outside the periodic interruption (47 ± 15 nm/s) plus the speed of cell edge retraction (49 ± 17 nm/s) was close to the bead speed during the periodic interruption (105 ± 26 nm/s; n = 16 events, 7 cells). This shows that interruptions resulted from a transient local increase in the retraction rate of the whole lamellipodial actin cytoskeleton, as the movement back of a cohesive structure.

Force Generation on Rigid Substrates Supports the Generation of Periodic Contractions

To verify that the generation of periodic contractions is dependent on the stiffness of the substrate and enables the cell to achieve full spreading (Wang et al., 2000), polarization, and migration (Lo et al., 2000; Mandeville et al., 1997), we tested the effects of the substrate rigidity on the generation of periodic contractions. We observed MEFs spreading on polyacrylamide gels of different stiffness coated with a constant FN concentration (Figures 2M–2P) (Lo et al., 2000; Wang et al., 2000). On stiff substrate (20% acrylamide, 0.8% bisacrylamide, Figure 2M), most cells (77 ± 12%, 43 cells, Figure 2P) generated periodic contractions having a period (23 ± 5 s; n = 136 events, 14 cells) not significantly different from cells spreading on FN-coated glass. In contrast, very soft substrate (10% acrylamide, 0.04% bisacrylamide, Figure 2O) neither supported the generation of periodic contractions nor effective protrusion of the leading edge, despite active actin rearward movement (100%, 12 cells, Figure 2P). Therefore, stiff substrates are needed for the generation of periodic contractions. Furthermore, even though an intermediary stiffness (10% acrylamide, 0.1% bisacrylamide, Figure 2N) restored an effective protrusion (90 ± 9%, 74 cells, Figure 2P) periodic contractions were observed only rarely (10 ± 15%, 74 cells, Figure 2P). Those protrusions were often not stabilized (52 ± 17%, 74 cells, Figure 2P), resulting in a global ruffling of the lamella. Hence, cell probing of a rigid substrate by contractile force generation results in periodic stabilization and extension cycles unlike less rigid substrates.

Periodic Contractions Trigger Transient Integrin β3 and Paxillin Clusters

If an increase in the retraction of actin causes stabilization of matrix interactions, then there may be accumulation of integrins and/or paxillin in a periodic array. We used β3-GFP integrin as a reporter for the formation of stronger edge contacts (Plancon et al., 2001) as well as paxillin-GFP (von Wichert et al., 2003). During the phase 1 of spreading, no visible integrin clusters were detected using TIRF microscopy (Figure 3A, first frames of the kymograph). However, during phase 2 of spreading we observed the formation of periodic rows of integrin clusters (Figure 3A, arrows and Figure 3D). The mean time between those rows is 23 ± 3 s (n = 67 intervals, 4 cells), is very close to the period we measured between interruptions (Figure 1). The distribution of distances between successive rows indicated a peak centered around 1150 nm (Figure 3C, n = 121 events, 3 cells), which is close to the mean distance reached by the leading edge after a single protrusion/retraction cycle (840 ± 520 nm, n = 65 events, 9 cells). Integrin clusters were immobile relative to the substrate (no rearward movements) and were unstable, lasting for about 2 min. During phase 3 of spreading, in cells displaying STEPs, larger adhesion sites, having the characteristics of focal adhesions, started to form. Their lifetime was longer compared to integrin rows and they displayed rearward movement. Thus, interruptions were concomitant with an increase in integrin density at the edge, which would strengthen the interaction with the substrate. No such row patterning was observed with cells expressing only GFP (Figure 3E), ruling out that variation of the cytoplasmic thickness, or the distance between the substrate and the cell was responsible for the observation.

If the increased retraction associated with the interruptions resulted in increased force on the integrins, then there should be an increase in the accumulation of GFP-paxillin (von Wichert et al., 2003). Indeed, GFP-paxillin formed the same row pattern as integrins (Figure 3B, arrows), and was also found in the focal adhesions that formed in phase 3 of spreading. Since GFP-paxillin does not accumulate at FN-bead sites unless force is applied, it appears that the increased retraction rate results in increased force being applied to the integrin contacts.

Inhibition of MLCK Affects Spreading and Periodic Contractions

Since periodic retractions of the lamellipodia are induced by force generation, we explored the effect of

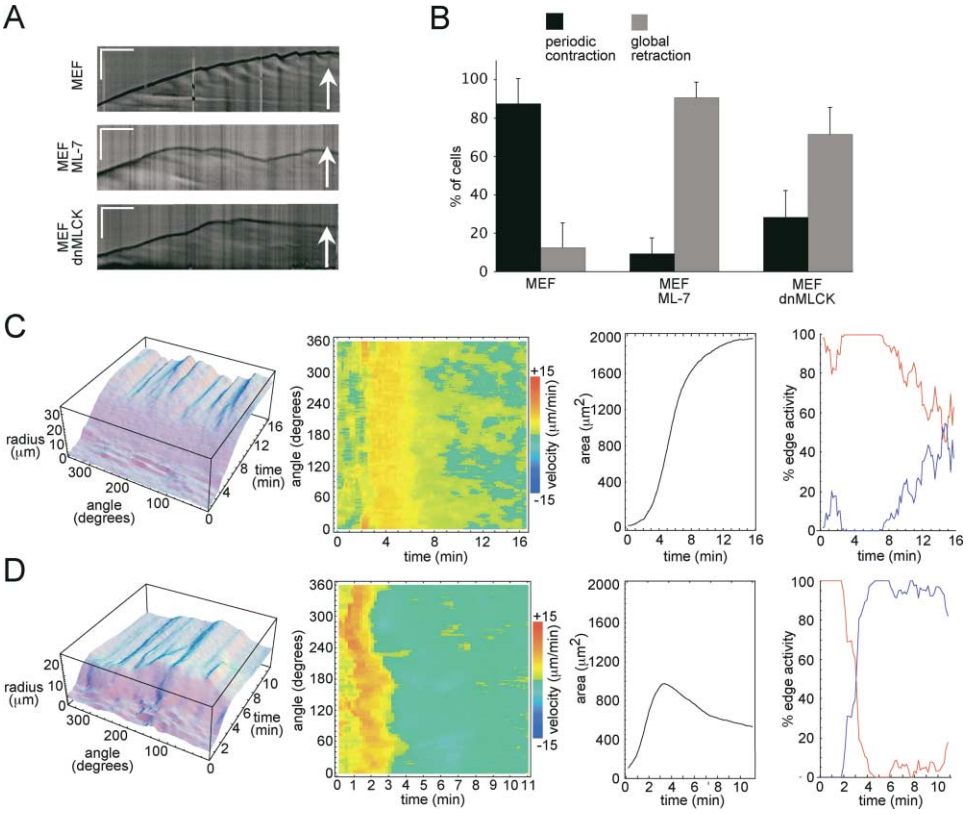

Figure 4. MLCK Affects the Generation of Periodic Contractions and the Spreading

(A) DIC kymographs of respectively, control MEF, ML-7-treated MEF, and dnMLCK-transfected MEF. Scale bars are equal to 4 μm. Time bars are equal to 30 s. Arrows indicate the direction of protrusion.

(B) Histogram representing the percentage of cells displaying periodic contractions (black), and global retraction (gray) for respectively, control MEF, ML-7-treated MEF, and dnMLCK-transfected MEF.

(C–D) Visualization of a control MEF (C) and ML-7 treated MEF (D) spreading. Radius as function of angle and time (left). Velocity maps (middle left). Variation of the cell area (middle right). Percent of edge activity (right). Note the global retraction following the phase 1 of spreading for (D). See Supplemental Movie S4 (available on *Cell* website) to better appreciate the transition between phase 1 and phase 2 of spreading.

modulating the contractile machinery of the cell. We tested if either inhibition of Rho kinase (ROCK) or MLCK affected the pattern of contractions. ROCK inhibition, using the specific inhibitor Y 27623 (25 μM), did not affect the generation of periodic contractions or the period (22 ± 4 s, n = 111 events, 14 cells) as observed in DIC experiments, but efficiently inhibited the formation of stress fibers (Supplemental Figure S3 available on *Cell* website). However, MLCK inhibition using the specific inhibitor ML-7 (10 μM) dramatically reduced the duration or canceled phase 2 of spreading without affecting phase 1 (only 9 ± 8% of cells showed a phase 2, n = 67 cells, Figure 4B) compared to control isotropic spreading cells (87 ± 13%, n = 62 cells, Figure 4B), as seen both in DIC (Figure 4A) and TIRF experiments (Figure 4D). Eventually, further spreading occurred, but in contrast to the extension/retraction cycles observed in phase 3 or anisotropic spreading, we observed fast protrusions interrupted by cessation of edge activity. Time-lapse analysis of MEFs spreading by TIRF (Figures 4C and 4D) demonstrated that 10 min after the initiation of spreading, ML-7 treated cells had a decreased area (790 ± 440 μm², n = 39 cells, Figure 4D, middle right) compared to untreated cells (2020 ± 1000 μm², n = 27 cells, Figure 4C, middle right). To further demonstrate MLCK involvement, we expressed a dominant-negative MLCK (dnMLCK) (see Experimental Procedures) (Figure 4A). Similarly to ML-7, dnMLCK expression inhibited phase 2 of spreading (28 ± 14% of control, n = 57 cells) (Figure 4B). Therefore, MLCK appears to be needed for increased force generated during periodic contractions and enables the cell to rapidly expand to a maximum area before polarization.

Periodic Contractions Induced the Periodic Transport of α-Actinin and MLCK from the Leading Edge to the Base of the Lamellipodium

Simultaneous with the interruption/retraction of the leading edge, we observed rearward moving material, visible as waves by DIC microscopy (Figure 5A). Analysis of wave movement revealed that the mean speed (74 ± 15 nm/s, n = 46 events, 4 cells) was similar to the speed of rearward moving FN-coated beads (~65 nm/s). Furthermore, the waves reached a distance of 1520 ± 250 nm from the leading edge (n = 48 events, 4 cells) when the next contraction was triggered, similar to the lamellipodial width of the MEFs used in our study (Figure 6C). These waves were probably actin structures, since the

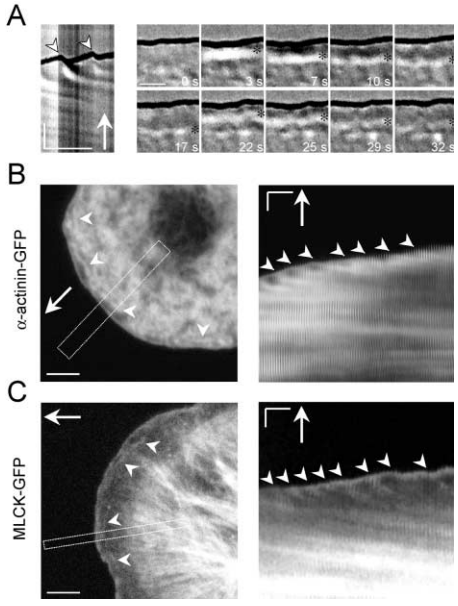

Figure 5. α-Actinin and MLCK Waves Travel across the Lamellipodium in Concert with Periodic Waves Triggered by Contractions

(A) DIC kymograph of a MEF spreading on FN 10 μg/ml showing the generation of waves by periodic contractions (left, arrowhead). Time-lapse sequence corresponding to the kymograph depicting the traveling of waves (stars) across the lamellipodia. Note that the generation of the next wave occurs when the first reaches the back region of the lamellipodium. Left: scale bars are equal to 2 μm. Time bar is equal to 30 s. Right: scale bars are equal to 2 μm. Arrows indicate the direction of protrusion.

(B–C) TIRF kymographs of MEFs expressing α-actinin-GFP (B) and MLCK-GFP (C) spreading on FN 10 μg/ml (right). The dotted rectangles in the left depict the regions used to generate the TIRF kymographs. Arrowheads indicate waves of α-actinin and MLCK-GFP moving across the lamellipodium. See Supplemental Movie S5A and S5B (available on *Cell* website) to better appreciate the generation of periodic α-actinin and MLCK waves and their movement across the lamellipodium during phase 2 of spreading. Left: scale bars are equal to 5 μm. Right: scale bars are equal to 2 μm. Time bars are equal to 30 s. Arrows indicate the direction of protrusion. Acquisition rate: α-actinin-GFP, 1 frame every 1 to 10 s; MLCK-GFP, 1 frame every 5 to 10 s.

actin binding protein α-actinin as observed by TIRF displayed the same periodic rearward movement during phase 2 of spreading (Figure 5B). The mean speed of moving α-actinin-GFP was 68 ± 27 nm/s (n = 31 events, 4 cells), and occurred every 23 ± 8 s (n = 20 events, 4 cells), similar to wave dynamics. Triggering of α-actinin movement from the edge started when the previous wave reached a distance of about 1640 ± 300 nm (n = 25 events, 4 cells) from the leading edge.

Because inhibition of MLCK affects the generation of interruption/retraction cycles and MLCK contains an actin binding site (Kamm and Stull, 2001), we studied its dynamics in the lamellipodia of MEFs transfected with MLCK-GFP (Poperechnaya et al., 2000) using TIRF (Figure 5C). Interestingly, periodic waves of MLCK were also observed, having a mean speed of 64 ± 23 nm/s (n = 25 events, 3 cells), occurring every 24 ± 7 s (n = 16 events, 3 cells) and reaching 1640 ± 170 nm from the leading edge at the time of the next cycle of MLCK movement (n = 17 events, 3 cells). Thus, MLCK waves, like α-actinin waves, chronicled the dynamics of actin filament waves generated by periodic contractions. The generation of α-actinin/MLCK rearward moving waves was distinct from the generation of immobile row patterning of integrin/paxillin, supporting the specificity of these observations. Furthermore, no such waves were observed with GFP expressing cells (Figure 3E).

Generation of Periodic Contractions Is Not Microtubule-Dependent but Is Linked to the Width of the Actin Meshwork

Periodic increases in contractile forces applied by the cell on the ECM may trigger periodic response signals but it is a mystery how the cycle could be timed. In the other case of periodic contractions, cortical oscillations in spreading cells were induced by depolymerization of microtubules (Pletjushkina et al., 2001). However, on the contrary to a global cortical oscillation, the contractions reported here are localized and not synchronized all around the spreading cell (Figure 1). Also, the specific ROCK inhibitor, Y-27632, did not suppress generation of localized contractions (Supplemental Figure S3 available on *Cell* website). In addition, depolymerization of microtubules with 1 mM nocodazole did not suppress periodic contractions (data not shown). Thus, the oscillating signal that controls contractions appears to be local and very different in nature from the global oscillations reported previously.

The leading lamellipodia in fibroblasts are supported by an extensively branched organization of actin filaments, termed the dendritic brush that is about 1 μm in width (Svitkina and Borisy, 1999). The mean width of the actin rich lamellipodia for MEFs used in our study was about 1500 nm (Figure 6C). At a mean speed of 50–70 nm/s (Figures 2 and 5), the time to move from the leading edge to the proximal boundary of lamellipodia is on the order of 20–30 s. If the period between interruptions was determined by the transport time, decreasing the width of the lamellipodia should decrease the time between interruptions. We modified the actin network in lamellipodia using low concentrations of cytochalasin D (CD) (50 nM) and latrunculin A (LA) (200 nM). At this concentration, CD preferentially caps the barbed ends, reducing the density of the lamellipodial actin network (Svitkina and Borisy, 1999). We also used LA, which sequesters G-actin monomers, under conditions that shifted the actin steady state toward depolymerization while not completely blocking motility. LA treatment induced narrowing of lamellipodia (Svitkina and Borisy, 1999). Cell edge protrusions analyzed by kymographs of CD-treated MEFs did not show a regular generation of interruptions. Instead, scarce interruptions were observed, despite a similar net movement of the edge (Figure 6B). In contrast, LA-treated cells still exhibited periodic interruptions, however the period between interruptions 18 ± 5 s (n = 92 events, 6 cells) was decreased compared to control MEFs 24 ± 7 s (Figure 6B). Clearly, the structure and dynamics of the actin meshwork affected the interruptions, and the period correlated with lamellipodial width.

Spreading Cells Regulate the Period of Contractions through Rac/LIMK/Cofilin Pathways

To test whether modification of the actin network dynamics by endogenous proteins altered the period be-

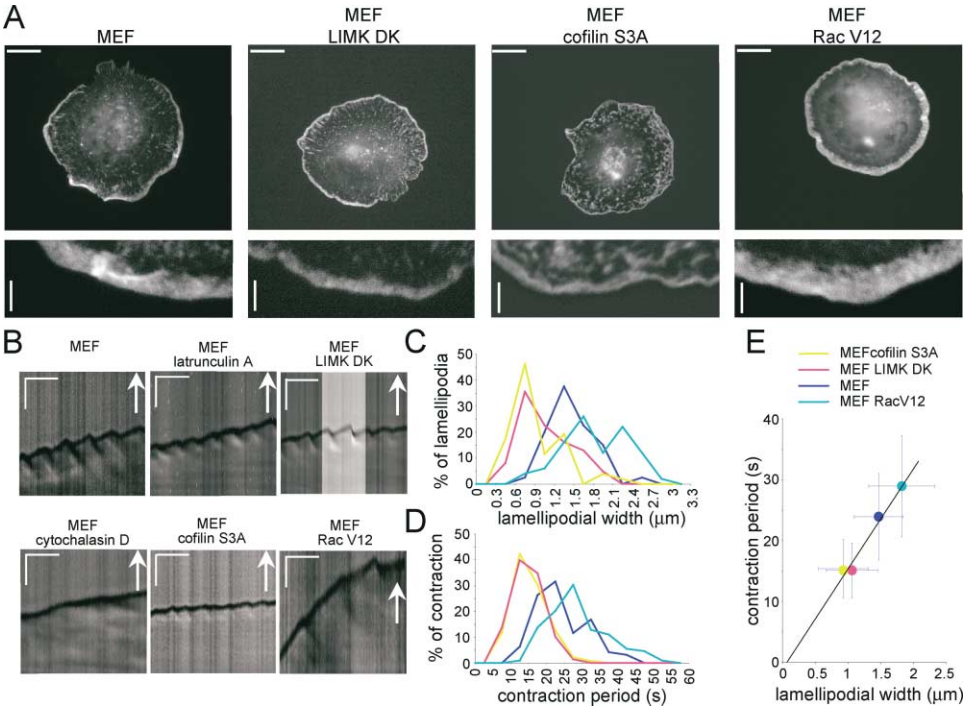

Figure 6. Rac/LIMK/Cofilin Signaling Pathway Affects the Periodicity of Interruption/Contraction in Spreading Cells

(A) Visualization of the lamellipodial width in MEFs transfected respectively with α-actinin-GFP, α-actinin-GFP, and LIMK DK; α-actinin-GFP and cofilin S3A; and α-actinin and RacV12. Scale bars are equal to 5 μm upper and 2 μm lower.

(B) DIC kymographs of a control MEF (upper left), CD-treated MEF (lower left), LA-treated MEF (upper middle), GFP and cofilin S3A-transfected MEF (lower middle), GFP and LIMK DK-transfected MEF (upper right), and GFP and RacV12-transfected MEF (lower right). See Supplemental Movies S6A (LA), S6B (cofilin S3A), S6C (LIMK DK), and S6D (RacV12) available on *Cell* website. Scale bars are equal to 2 μm. Time bars are equal to 30 s. Arrows indicate the direction of protrusion.

(C) Distribution of the lamellipodial widths in MEFs transfected respectively with α-actinin-GFP (dark blue); α-actinin-GFP and LIMK DK (pink); α-actinin-GFP and cofilin S3A (yellow); and α-actinin and RacV12 (light blue). Note the lamellipodial width decrease in LIMK DK and cofilin S3A-transfected MEFs, and increase in RacV12-transfected MEFs, compared to control MEFs. Lamellipodial width distributions are significantly different between control, RacV12, and LIMK DK/cofilin S3A ($p < 0.001$, Bonferroni post hoc test), while no significant difference was found between LIMK DK and cofilin S3A.

(D) Distribution of the contraction periods in control MEFs (dark blue), GFP and LIMK DK-transfected MEFs (pink), GFP and cofilin S3A-transfected MEFs (yellow), and GFP and RacV12-transfected MEFs (light blue). Note the contraction period decrease in LIMK DK and cofilin S3A-transfected MEFs, and increase in RacV12-transfected MEFs, compared to control MEFs. The distributions of contraction periods are significantly different between control, RacV12, and LIMK DK/cofilin S3A ($p < 0.001$, Bonferroni post hoc test) while no significant difference was found between LIMK DK and cofilin S3A.

(E) Linear relationship between the lamellipodial width and the contraction period (correlation coefficient $R^2 = 0.97$).

tween contractions, we modified cofilin activity. There is an inverse relationship between the amount of active cofilin and Listeria actin tail lengths in vitro (Carlier et al., 1997; Rosenblatt et al., 1997). Thus, cofilin activation might decrease, whereas, inactivation of cofilin by LIM kinase phosphorylation might increase the width of lamellipodia (Arber et al., 1998; Yang et al., 1998). We activated ADF/cofilin by transfecting MEFs with a dominant-negative LIMK1 (LIMK DK) or with an active non-phosphorylatable mutant of cofilin (cofilin S3A), and inactivated cofilin by transfecting MEFs with a constitutively active Rac GTPase (RacV12) (Arber et al., 1998). Enhanced cofilin activity induced a decrease in the period between contractions (15 ± 5 s) for LIMK DK (n = 138 events, 7 cells) and cofilin S3A (n = 135 events, 11 cells) (Figures 6B and 6D). Conversely, RacV12 induced an increase in the period (29 ± 8 s, n = 109 events, 13 cells) (Figures 6B and 6D). Furthermore, decreased and increased periods were correlated respectively with a narrower and wider lamellipodial width, as measured using α-actinin-EGFP (Figures 6A and 6C). Increased cofilin activity in LIMK DK and cofilin S3A transfected cells reduced the mean lamellipodial width respectively to 1060 ± 390 nm (n = 62 cells) and 930 ± 380 nm (n = 52 cells) compared to control MEFs 1470 ± 370 nm (n = 40 cells), and constitutively active RacV12 increased the lamellipodial width to 1820 ± 500 nm (n = 50 cells). ROCK inhibition, which did not affect significantly the period compared to control cells (22 ± 4 s, n = 111 events, 14 cells), did not affect significantly the lamellipodial width (1510 ± 310 nm, n = 61 cells) (Supplemental Figure S3 available on *Cell* website). The relationship between the period and the lamellipodial width is linear (Figure 6E) and passes through the origin within experimental error. Thus, there appears to be no time delay between contractions and the initiation of the contractile signal movement at the cell edge.

Discussion

The periodic interruptions in the edge extension during spreading and migration are linked to an increased con-

traction of the lamellipodial F-actin as evidenced by the increased rate of rearward transport of FN-coated beads and the periodic formation of integrin/paxillin rows. It appears that periodic contractions are used by the cell to promote further extension of lamellipodia without filopodia on substrates of adequate rigidity, as shown by the reduced spread area after MLCK inhibition and unstable lamellipodia on soft substrates. Because adjacent regions of the lamellipodium show contractions that are offset in time but have the same period, there appears to be local control of the contractions that involves slow moving components. Since signals can be generated at matrix-cytoskeleton binding sites by contractile force, it is logical to postulate that the signal could also bind to the actin filaments and be carried rearward. MLCK and α-actinin are carried from the leading edge to the back of lamellipodia in approximately 25 s, which is the period between contractions. As the width of the lamellipodium decreases or increases, the period decreases or increases proportionally. Therefore, our study supports the hypothesis that proteins bound to the actin locally deliver the signal for increased contractility and directed actin assembly.

Periodic Contractions in the Protrusive Lamellipodia May Be Linked to Mechanical Probing of the Substrate

To probe its environment, the cell uses directional actin assembly to extend the membrane (Pantaloni et al., 2001; Pollard and Borisy, 2003; Small et al., 2002) and generates protrusive forces with lamellipodial extension (Munevar et al., 2001). The generation of periodic contractions requires rigid substrates and is associated with stabilization of protruding lamellipodia without filopodia. Therefore, we suggest that generation of periodic contractions in extended lamellipodia is linked to the mechanical probing of the ECM rigidity by the cell. In such a model, rigid substrates that promote the generation of periodic contractions will induce stabilization of the protrusive lamellipodia and movement of the cell toward rigid regions (Lo et al., 2000). At a molecular level, forces applied on ECM-integrin-actin connections trigger signals needed for their stabilization and accumulation of focal complex proteins (Choquet et al., 1997; Galbraith et al., 2002; Giannone et al., 2003; von Wichert et al., 2003). If this contractile signal activated by local force is carried rearward on the actin, then stiffer regions would induce a stronger contractile response. Indeed, soft substrates did not support the generation of periodic contractions and protrusions of the lamellipodia. This positive feedback loop would naturally cause the cell to move toward more rigid matrices (Lo et al., 2000). As an extension of this hypothesis, the surface area of cells spreading on a soft substrate is decreased compared to a stiff substrate (Wang et al., 2000), and MLCK inhibition reduced the final area of the spreading cells. Therefore, integrin binding to rigid matrices and the generation of a local contractile signal can generate a signal to direct actin assembly during cell locomotion.

Cycles of Protrusion and Contraction May Link Actin Polymerization to Adhesion Site Formation

Extension of cell processes does not require interaction of integrins with the ECM, since filopodia and lamellipodia extend in the presence of adhesion-blocking peptides and over nonadhesive surfaces (Bailly et al., 1998). However, without effective binding and mechanical stabilization, forward movements of the leading edge fold back upon themselves, leading to ruffling and no net increase in the cell-surface contact area. We demonstrated that phase 1 of fibroblast spreading did not involve extensive contractions or adhesion site formation. However, during phase 2 and migration, productive extension requires coupling of the actin meshwork assembly to force generation on integrins, as previously suggested (Mitchison and Cramer, 1996; Sheetz et al., 1998). Force generation is necessary for the accumulation of talin, paxillin, and vinculin leading to stable interaction with the actin cytoskeleton (Galbraith et al., 2002; Giannone et al., 2003) and possibly actin polymerization since vinculin recruits the Arp2/3 complex (DeMali et al., 2002).

Protrusion is powered by forward forces generated on the membrane while adhesion site formation results from rearward forces applied on the ECM. Because these forces are in opposition, periodic contractions may provide an effective way to couple protrusion with stabilization of the cell edge leading to an increase in the cell contact area. Observations suggesting that firm adhesion sites form in response to contraction preferentially at tips of lamellipodia are: (1) the leading edge has high-affinity integrin readily available to form new adhesion sites (Kiosses et al., 2001; Nishizaka et al., 2000); (2) lamellipodial tips that do not bind to the surface often ruffle, leaving the cell edge at the position it reached at the time of the previous periodic contraction; and (3) the distance and period between integrin rows corresponds to the generation of periodic contractions. Even lamellipodia with filopodia that do not generate periodic contractions but instead rounds of protrusion and retraction indicate that protrusion/contraction cycles may be a general mechanism to explore the environment.

Signals Traveling on Actin Filaments

The local response to force on matrix contacts involves the fast accumulation of focal complex proteins at the site of force generation and the subsequent transport rearward of the material with the actin cytoskeleton (i.e., FN-coated beads) (Galbraith et al., 2002; von Wichert et al., 2003). If the matrix contact is immobilized (i.e., FN-coated glass), a portion of the actin cytoskeleton proteins will remain with the matrix contact (integrin, paxillin) whereas others will move with the F-actin (MLCK, α-actinin). Therefore, it is possible that signaling complexes activated by force at localized sites are transported radially by actin rearward flow to downstream targets. Our study supports this concept of cytoskeletal transport of bound signaling complexes.

First, the fact that adjacent regions of the lamellipodium show contractions that are offset in time but have the same period strongly favors models where contractions are controlled by bound complexes. Diffusion in cytoplasm is relatively rapid such that soluble signals, even proteins, could diffuse over tens of microns in the twenty or more seconds between contractions and blur lateral boundaries. In contrast, the radial movements

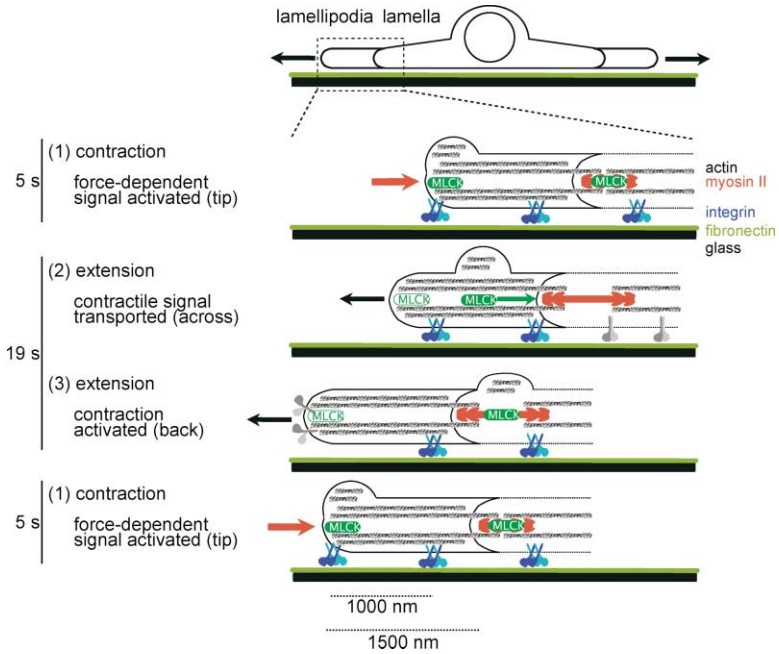

Figure 7. Model of Signaling by Cytoskeletal Transport

Schematic drawing depicting how cytoskeletal transport of a contractile signal generates local, periodic cycles of contraction.

(1) Lamellipodial contraction generates force that activates a force-dependent signal, including MLCK (green ellipses), bound to actin at the lamellipodial tip. Note the formation of transient integrin/paxillin adhesion sites at the tip (blue); the partial dissociation of the actin meshwork creating a wave (bulges) that is carried rearward.

(2) Extension resumes after the contraction, since the rate of actin rearward movement becomes inferior to filament assembly rate. The wave of material (actin, α-actinin, MLCK) containing the contractile signal is transported rearward by actin flow from the tip to the back of the lamellipodium.

(3) The activated signaling complex reaches the back of the lamellipodium, where it now stimulates the activation of the contractile machinery (myosin II, red). Once the contraction is activated, the next cycle begins.

of the actin cytoskeleton are confined and could carry signals that arise from local matrix properties in a radial fashion.

Second, the time for transport across lamellipodia seems to control the period of the contraction cycles because several different treatments that alter the width of lamellipodia alter the period between contractions. Accordingly, a linear relationship was found between the width of the lamellipodia actin network and the period of retraction, whereas the time for diffusion of signals depends on the square of the distance.

Thus, we suggest that actin filaments carry the signaling complexes from the leading edge to the proximal region, as observed for DIC waves, α-actinin, and MLCK, where they locally activate the next round of myosin contraction (Figure 7). Although, depolymerization of F-actin occurs throughout the lamellipodia (Svitkina and Borisy, 1999; Watanabe and Mitchison, 2002), at the proximal boundary of lamellipodia, actin filaments are extensively dissociated and remodeled, probably releasing the components bound to them (Pollard and Borisy, 2003). An alternative hypothesis is that enzymes at the proximal edge of the lamellipodium activate the release. The same hypotheses can explain the finding that FN-coated beads bind preferentially at the leading edge, move rearward with the actin cytoskeleton to the proximal boundary of lamellipodia, and often release from the membrane at that point (Nishizaka et al., 2000). Thus, there is prior evidence of protein transport by binding at the leading edge, movement with the actin filaments and release at the proximal boundary of the lamellipodia.

Is MLCK the Signal?

In such a complicated process, it is unlikely that MLCK transport alone controls the period of contractions. However, the function, location, and dynamics of MLCK are those expected for a protein that would control contractile activity in a cytoskeleton transport-signaling pathway. Specific inhibition of MLCK by ML-7 or dnMLCK inhibits the generation of periodic contractions. The only known physiological substrate for MLCK is myosin regulatory light chain (RLC), and phosphorylation on Ser 19 of the myosin II RLC regulates actomyosin contractility leading to cytoskeleton and adhesion site remodeling during cell migration (Kamm and Stull, 2001). In addition, in phase 2 of spreading, MLCK-GFP is bound to the lamellipodial edge, suggesting that periodic contractions release a fraction of this MLCK that will be transported as periodic waves with actin filaments as observed in our study. A recent study demonstrated that MLCK is active in lamellipodia (Chew et al., 2002). However, the Ser19 phosphorylated form of myosin II RLC is mostly concentrated at the back of the lamellipodia (Matsumura et al., 1998). Therefore, MLCK activation of myosin II concentrated at the back of the lamellipodia (Verkhovsky et al., 1995) could cause the concerted movement of the lamellipodia.

Our study of the periodic contractions of lamellipodia without filopodia in spreading and migrating cells leads us to propose that signal transduction by cytoskeletal transport may be a more general mechanism. Soluble second messengers or signaling enzymes are mostly diffusive and cause modification of downstream targets in all directions. In contrast, signals that are transported on the cytoskeleton move in a directed fashion and can provide a simple mechanism for a positional signal leading to local protrusion and contraction. Thus, cellular contacts with even small regions of a given matrix can produce directed movements and responses using myosin and other components that are widely dispersed throughout the cell. This could be an important general mechanism to convert the rigidity of specific matrices into signals for tissue differentiation and morphology determination.

Experimental Procedures

Cell Culture

Immortalized MEFs (von Wichert et al., 2003) were cultured in DMEM (Gibco) with 10% FBS. One day prior to experiments, cells were sparsely plated to minimize cell-cell interactions prior to replating. Transient transfection of plasmids encoding EGFP (Clontech, Palo Alto, CA), paxillin-GFP, α-actinin-EGFP (provided by C.A. Otey, Department of Cell and Molecular Physiology, University of North Carolina, Chapel Hill), avian long MLCK-EGFP (Poperechnaya et al., 2000), integrin β3-EGFP (Plancon et al., 2001), dnMLCK, LIMK DK, cofilin S3A, and RacV12 (Arber et al., 1998) were performed with Fugene 6 (Roche). The 220 kDa mouse MLCK was cloned from a mouse AT2 cardiomyocytes (Blue et al., 2002) and a single point mutation was introduced at residue 1549 (K1549A). This mutation is predicted by alignment with other ser/thr kinases to have a key role in binding ATP and has been previously shown to inactivate MLCK activity thereby rendering it a dominant-negative, kinase-dead enzyme (Jin et al., 2001).

Materials

Calcein-AM was purchased from Molecular Probes, Inc. Full-length human fibronectin was purchased from Roche. Hexamethyl disilazane (HMDS), LA, CD, and nocodazole was purchased from Sigma. ROCK inhibitor (Y-27632) and MLCK inhibitor (ML-7) was purchased from Tocris.

Coverglass Preparation

Coverglasses were acid washed and treated with HMDS, creating a hydrophobic surface preventing nonspecific receptor activation. This surface was exposed to a 200 μl layer of 10 μg/ml FN solution for 1 hr at 37°C. The uniformity of protein coating was confirmed by observation of Cy-5-labeled ECM. The preparation of polyacrylamide substrates of different rigidity covalently coated with FN was performed as described previously (Lo et al., 2000; Wang et al., 2000).

Spreading Assays

Cells were detached with trypsin/EDTA (0.05% for 2 min), the trypsin inactivated with soy bean trypsin inhibitor (1 mg/ml in DMEM), the cells suspended in serum free condition in DMEM, and incubated for 30 min before plating on coated glass surface. For ML-7, Y-27632, LA, CD, and nocodazole experiments, cells were preincubated for 30 min and during the experiments. When cells were transfected with a plasmid encoding a protein not fused to GFP, GFP was transiently cotransfected to localize transfected cells.

Total Internal Reflection Fluorescence Microscopy

Cells were loaded with 0.2 μM of Calcein AM for 30 min before trypsinization or transfected with a GFP fusion protein. We built a custom-designed prism-based TIRF microscope using an upright Olympus BX-50 microscope coupled to the 488 nm excitation light from a Melles Griot argon-ion laser. Cells were visualized respectively with a 20× and 60× water immersion objectives for Calcein and GFP experiments. A Roper Scientific CoolSnap fx cooled CCD camera recorded 16 bit digital grayscale images from the microscope.

Laser Trap Experiments

Cells were seeded on ECM coated coverglass and visualized with a 1.3 NA 100× plan-neofluar objective on an inverted microscope, Axiovert 100 TV, equipped with differential interference contrast optics as previously described (Choquet et al., 1997). 0.64 μm silica beads (Bang laboratory) were coated with FN trimer as described previously (Giannone et al., 2003). FN-coated beads were sequentially held on the cell surface at the leading edge using a 100 mW (20 pN/μm) optical-gradient laser trap setup (Zeiss Axiovert 100TV) while the cell was spreading.

Image Analysis

Individual fluorescent TIRF images of a spreading cell were processed as described elsewhere (Dubin-Thaler et al., 2004) with a custom java image segmenter, resulting in a curve differentiating the edge of the cell from the background. Further analysis was done using Mathematica (Wolfram Research, Inc.) software as described elsewhere (Dubin-Thaler et al., 2004).

TIRF time lapse was performed as described above and digitized as indicated in figure legend. Kymographs were produced and analyzed using ImageJ software. Kymographs were generated by putting side by side thin (10–20 pixels) radial regions of the spreading cell in a time-lapse sequence.

DIC time-lapse sequences were obtained at video rate using the same experimental setup described for laser trap experiments. Movies were digitized at 3 Hz. The cell edge was determined by a local contour algorithm (Döbereiner et al., 1997) allowing nanometer spatial resolution. Further analysis was done using Mathematica (Wolfram Research, Inc.) software as described elsewhere (Dubin-Thaler et al., 2004).

Statistical Analysis

All statistical analyses were performed with a Bonferroni post hoc test. Linear fits were found using a least squares fit to the data.

Acknowledgments

We are very grateful to Patricia Gallagher and Audrey Minden for providing us with respectively the dnMLCK and cofilin S3A, LIMK DK constructs. We thank Ravi Iyengar and Kyle Miller for helpful discussion and for comments on the manuscript. This work was supported by NIH grant GM362.

Received: July 14, 2003
Revised: November 26, 2003
Accepted: December 9, 2003
Published: February 5, 2004

References

Arber, S., Barbayannis, F.A., Hanser, H., Schneider, C., Stanyon, C.A., Bernard, O., and Caroni, P. (1998). Regulation of actin dynamics through phosphorylation of cofilin by LIM-kinase. Nature *393*, 805–809.

Bailly, M., Yan, L., Whitesides, G.M., Condeelis, J.S., and Segall, J.E. (1998). Regulation of protrusion shape and adhesion to the substratum during chemotactic responses of mammalian carcinoma cells. Exp. Cell Res. *241*, 285–299.

Bear, J.E., Svitkina, T.M., Krause, M., Schafer, D.A., Loureiro, J.J., Strasser, G.A., Maly, I.V., Chaga, O.Y., Cooper, J.A., Borisy, G.G., and Gertler, F.B. (2002). Antagonism between Ena/VASP proteins and actin filament capping regulates fibroblast motility. Cell *109*, 509–521.

Blue, E.K., Goeckeler, Z.M., Jin, Y., Hou, L., Dixon, S.A., Herring, B.P., Wysolmerski, R.B., and Gallagher, P.J. (2002). 220- and 130-kDa MLCKs have distinct tissue distributions and intracellular localization patterns. Am. J. Physiol. Cell Physiol. *282*, C451–C460.

Bokel, C., and Brown, N.H. (2002). Integrins in development: moving on, responding to, and sticking to the extracellular matrix. Dev. Cell *3*, 311–321.

Cameron, L.A., Giardini, P.A., Soo, F.S., and Theriot, J.A. (2000). Secrets of actin-based motility revealed by a bacterial pathogen. Nat. Rev. Mol. Cell Biol. *1*, 110–119.

Carlier, M.F., Laurent, V., Santolini, J., Melki, R., Didry, D., Xia, G.X., Hong, Y., Chua, N.H., and Pantaloni, D. (1997). Actin depolymerizing factor (ADF/cofilin) enhances the rate of filament turnover: implication in actin-based motility. J. Cell Biol. *136*, 1307–1322.

Chew, T.L., Wolf, W.A., Gallagher, P.J., Matsumura, F., and Chisholm, R.L. (2002). A fluorescent resonant energy transfer-based biosensor reveals transient and regional myosin light chain kinase activation in lamella and cleavage furrows. J. Cell Biol. *156*, 543–553.

Choquet, D., Felsenfeld, D.P., and Sheetz, M.P. (1997). Extracellular matrix rigidity causes strengthening of integrin-cytoskeleton linkages. Cell *88*, 39–48.

Cramer, L.P., and Mitchison, T.J. (1995). Myosin is involved in postmitotic cell spreading. J. Cell Biol. *131*, 179–189.

DeMali, K.A., Barlow, C.A., and Burridge, K. (2002). Recruitment of the Arp2/3 complex to vinculin: coupling membrane protrusion to matrix adhesion. J. Cell Biol. *159*, 881–891.

Döbereiner, H.G., Evans, E., Kraus, M., Seifert, U., and Wortis, M. (1997). Mapping vesicle shapes into the phase diagram: a comparison of experiment and theory. Phys. Rev. *E55*, 4458–4474

Dubin-Thaler, B.J., Giannone, G., Döbereiner, H.G., and Sheetz, M.P. (2004). Nanometer analysis of cell spreading on matrix-coated surfaces reveals two distinct cell states and STEPs. Biophys. J., in press.

Galbraith, C.G., Yamada, K.M., and Sheetz, M.P. (2002). The relationship between force and focal complex development. J. Cell Biol. *159*, 695–705.

Giannone, G., Jiang, G., Sutton, D.S., Critchley, D.R., and Sheetz, M.P. (2003). Talin1 is critical for force-dependent reinforcement of initial integrin-cytoskeleton bonds but not tyrosine kinase activation. J. Cell. Biol. *163*, 409–419.

Gillespie, P.G., and Walker, R.G. (2001). Molecular basis of mechanosensory transduction. Nature *413*, 194–202.

Huang, S., and Ingber, D.E. (1999). The structural and mechanical complexity of cell-growth control. Nat. Cell Biol. *1*, E131–E138.

Jin, Y., Atkinson, S.J., Marrs, J.A., and Gallagher, P.J. (2001). Myosin ii light chain phosphorylation regulates membrane localization and apoptotic signaling of tumor necrosis factor receptor-1. J. Biol. Chem. *276*, 30342–30349.

Kamm, K.E., and Stull, J.T. (2001). Dedicated myosin light chain kinases with diverse cellular functions. J. Biol. Chem. *276*, 4527–4530.

Kiosses, W.B., Shattil, S.J., Pampori, N., and Schwartz, M.A. (2001). Rac recruits high-affinity integrin alphavbeta3 to lamellipodia in endothelial cell migration. Nat. Cell Biol. *3*, 316–320.

Lappalainen, P., and Drubin, D.G. (1997). Cofilin promotes rapid actin filament turnover in vivo. Nature *388*, 78–82.

Lo, C.M., Wang, H.B., Dembo, M., and Wang, Y.L. (2000). Cell movement is guided by the rigidity of the substrate. Biophys. J. *79*, 144–152.

Loisel, T.P., Boujemaa, R., Pantaloni, D., and Carlier, M.F. (1999). Reconstitution of actin-based motility of Listeria and Shigella using pure proteins. Nature *401*, 613–616.

Mandeville, J.T., Lawson, M.A., and Maxfield, F.R. (1997). Dynamic imaging of neutrophil migration in three dimensions: mechanical interactions between cells and matrix. J. Leukoc. Biol. *61*, 188–200.

Matsumura, F., Ono, S., Yamakita, Y., Totsukawa, G., and Yamashiro, S. (1998). Specific localization of serine 19 phosphorylated myosin II during cell locomotion and mitosis of cultured cells. J. Cell Biol. *140*, 119–129.

Miki, H., Yamaguchi, H., Suetsugu, S., and Takenawa, T. (2000). IRSp53 is an essential intermediate between Rac and WAVE in the regulation of membrane ruffling. Nature *408*, 732–735.

Mitchison, T.J., and Cramer, L.P. (1996). Actin-based cell motility and cell locomotion. Cell *84*, 371–379.

Munevar, S., Wang, Y.L., and Dembo, M. (2001). Distinct roles of frontal and rear cell-substrate adhesions in fibroblast migration. Mol. Biol. Cell *12*, 3947–3954.

Nishizaka, T., Shi, Q., and Sheetz, M.P. (2000). Position-dependent linkages of fibronectin-integrin-cytoskeleton. Proc. Natl. Acad. Sci. USA *97*, 692–697.

Pantaloni, D., Le Clainche, C., and Carlier, M.F. (2001). Mechanism of actin-based motility. Science *292*, 1502–1506.

Parker, K.K., Brock, A.L., Brangwynne, C., Mannix, R.J., Wang, N., Ostuni, E., Geisse, N.A., Adams, J.C., Whitesides, G.M., and Ingber, D.E. (2002). Directional control of lamellipodia extension by constraining cell shape and orienting cell tractional forces. FASEB J. *16*, 1195–1204.

Plancon, S., Morel-Kopp, M.C., Schaffner-Reckinger, E., Chen, P., and Kieffer, N. (2001). Green fluorescent protein (GFP) tagged to the cytoplasmic tail of alphaIIb or beta3 allows the expression of a fully functional integrin alphaIIb(beta3): effect of beta3GFP on alphaIIb(beta3) ligand binding. Biochem. J. *357*, 529–536.

Pletjushkina, O.J., Rajfur, Z., Pomorski, P., Oliver, T.N., Vasiliev, J.M., and Jacobson, K.A. (2001). Induction of cortical oscillations in spreading cells by depolymerization of microtubules. Cell Motil. Cytoskeleton *48*, 235–244.

Pollard, T.D., and Borisy, G.G. (2003). Cellular motility driven by assembly and disassembly of actin filaments. Cell *112*, 453–465.

Poperechnaya, A., Varlamova, O., Lin, P.J., Stull, J.T., and Bresnick, A.R. (2000). Localization and activity of myosin light chain kinase isoforms during the cell cycle. J. Cell Biol. *151*, 697–708.

Rohatgi, R., Ma, L., Miki, H., Lopez, M., Kirchhausen, T., Takenawa, T., and Kirschner, M.W. (1999). The interaction between N-WASP and the Arp2/3 complex links Cdc42-dependent signals to actin assembly. Cell *97*, 221–231.

Rosenblatt, J., Agnew, B.J., Abe, H., Bamburg, J.R., and Mitchison, T.J. (1997). Xenopus actin depolymerizing factor/cofilin (XAC) is responsible for the turnover of actin filaments in Listeria monocytogenes tails. J. Cell Biol. *136*, 1323–1332.

Sawada, Y., and Sheetz, M.P. (2002). Force transduction by Triton cytoskeletons. J. Cell Biol. *156*, 609–615.

Sheetz, M.P., Wayne, D.B., and Pearlman, A.L. (1992). Extension of filopodia by motor-dependent actin assembly. Cell Motil. Cytoskeleton *22*, 160–169.

Sheetz, M.P., Felsenfeld, D.P., and Galbraith, C.G. (1998). Cell migration: regulation of force on extracellular-matrix-integrin complexes. Trends Cell Biol. *8*, 51–54.

Small, J.V., Stradal, T., Vignal, E., and Rottner, K. (2002). The lamellipodium: where motility begins. Trends Cell Biol. *12*, 112–120.

Svitkina, T.M., and Borisy, G.G. (1999). Arp2/3 complex and actin depolymerizing factor/cofilin in dendritic organization and treadmilling of actin filament array in lamellipodia. J. Cell Biol. *145*, 1009–1026.

Verkhovsky, A.B., Svitkina, T.M., and Borisy, G.G. (1995). Myosin II filament assemblies in the active lamella of fibroblasts: their morphogenesis and role in the formation of actin filament bundles. J. Cell Biol. *131*, 989–1002.

von Wichert, G., Jiang, G., Kostic, A., De Vos, K., Sap, J., and Sheetz, M.P. (2003). RPTP-alpha acts as a transducer of mechanical force on alphav/beta3-integrin-cytoskeleton linkages. J. Cell Biol. *161*, 143–153.

Wang, H.B., Dembo, M., and Wang, Y.L. (2000). Substrate flexibility regulates growth and apoptosis of normal but not transformed cells. Am. J. Physiol. Cell Physiol. *279*, C1345–C1350.

Watanabe, N., and Mitchison, T.J. (2002). Single-molecule speckle analysis of actin filament turnover in lamellipodia. Science *295*, 1083–1086.

Yang, N., Higuchi, O., Ohashi, K., Nagata, K., Wada, A., Kangawa, K., Nishida, E., and Mizuno, K. (1998). Cofilin phosphorylation by LIM-kinase 1 and its role in Rac-mediated actin reorganization. Nature *393*, 809–812.